Coherent control of electron spin dynamics in nano-engineered semiconductor structures

Denega, Sergii Zinoviyovych

Chapter 5

Spin-dephasing anisotropy for electrons in a quasi-1D GaAs wire without quantum confinement

Abstract

We present a numerical study of the electron-spin dephasing time T_2^* in quasi-ballistic wires of bulk GaAs material. The study assumes that dephasing occurs due to spin-orbit fields from a bulk Dresselhaus term and a Rashba term in wires with specular momentum scattering on the walls. With a similar magnitude for the Dresselhaus and Rashba effect our results show the longest T_2^* values for wires in [110] direction. This is consistent with the dependence of T_2^* on the crystal orientation of wires that was observed in recent experiments. However, a comparison with results for random momentum scattering on the wire edges reveals that the mechanism behind the spin dephasing anisotropy differs from the analogues effect in wires with two-dimensional electron systems. We also studied the magnetic field dependence of this phenomenon with simulations that account for the field-induced cyclotron motion of electrons.

This chapter is based on Ref. 1 on p. 103.

5.1 Introduction

The spin dephasing of mobile electron ensembles in III-V semiconductors such as GaAs occurs predominantly due to spin precession in spin-orbit fields. These spin-orbit fields are highly anisotropic in momentum space, such that random electron motion within an ensemble results in random precession [1, 2]. For two-dimensional (2D) electron ensembles in quantum wells the spin-orbit effect can be dominated by two terms (see Ref [2] for details): the linear Dresselhaus term (due to a lack of inversion symmetry in the crystal structure) and the Rashba term (due to the inversion symmetry breaking that is associated with the quantum well structure). Such systems can be engineered to give zero spin-orbit fields for electrons with k-vectors along the [110] direction [3]. This has been central in many theoretical proposals [4, 2, 5, 6, 7, 8] aimed at suppressing spin dephasing. Such a suppression has been observed with quasi-1D wire systems based on 2D GaAs materials [3, 9, 10], where the spin dephasing time showed a dependence on the crystal orientation in the wires.

One of these experiments also showed the unexpected result that the spin dephasing time T_2^* for electrons in wires based on bulk GaAs also has a dependence on the crystal orientation in the wires [10]. Also here, the longest T_2^* values were observed for wires along the [110] direction. Initial numerical studies of this effect that were reported in the original publication on the experiment indicated that the spin dephasing anisotropy (SDA) in these wires also relies on a cancelation between to spin-orbit terms. In this case, these are the cubic Dresselhaus [11] term and the Rashba term [12]. While the Rashba term is mostly described in the context of 2D electron systems, for micron-thick bulk layers it can also play a role. In the reported experiment there was an unidirectional electric field present in a micron-thick bulk layer near the wafer surface due to band-bending.

We report here further numerical studies on this effect for bulk electrons in quasi-ballistic GaAs wires. In particular, we report a more detailed study of the magnetic field dependence of these effects by including the effect of the external magnetic field on the electron trajectories. While this can be neglected for 2D electron systems with in-plane field, for bulk systems the cyclotron-motion effects are very significant. In addition, we compared in our studies the case of specular and random momentum scattering on the walls of the wires. This revealed that the mechanism behind the spin dephasing anisotropy in wires with specular scattering differs from the analogues effect in wires with 2D electron systems. Instead of a confinement-induced motional-narrowing effect, spin dephasing anisotropy

now results from the interplay between repetitive electron trajectories in the wire and the anisotropy in the spin orbit fields. This points to a mechanism that has similarities with the phenomenon of ballistic spin resonance that can occur in wires based on 2D electron systems [13].

5.2 Spin-orbit coupling

For convenience we describe the spin-orbit (SO) coupling as a k-vector dependent effective magnetic field which acts on the spin of an electron. For III-V semiconductors with zinc-blende crystal structure the SO coupling was derived by G. Dresselhaus [11] and can be expressed in the following form [12]:

$$\vec{B}_D^{bulk} = (2\gamma/g\mu_B)\left[\hat{x}k_x(k_y^2 - k_z^2) + \hat{y}k_y(k_z^2 - k_x^2) + \hat{z}k_z(k_x^2 - k_y^2)\right], \tag{5.1}$$

where μ_B is the Bohr magneton, g is the g factor for an electron in the conduction band and γ is the strength of the SO interaction. The link to the crystallographic axes is represent by the unit vectors $\hat{x}$, $\hat{y}$ and $\hat{z}$ which are in the directions [100], [010] and [001], respectively.

For the two-dimensional case with quantum confinement along the z direction in a quantum well of width a, $\langle k_z \rangle = 0$. However, the electrons are then in a state with a very significant value for $\langle k_z^2 \rangle \approx (\pi/a)^2$. The Dresselhaus SO field can then be expressed in the form of two terms with a different power dependence on k. It yields the linear Dresselhaus term, which dominates in the limit of $(\pi/a)^2 \gg k_x^2 + k_y^2$,

$$\vec{B}_{D1} = (2\gamma/g\mu_B)\left(\frac{\pi}{a}\right)^2 [-\hat{x}k_x + \hat{y}k_y]. \tag{5.2}$$

The cubic Dresselhaus term for the case of such a quantum well system is

$$\vec{B}_{D3} = (2\gamma/g\mu_B)\left[\hat{x}k_x k_y^2 - \hat{y}k_y k_x^2\right]. \tag{5.3}$$

The value for the coupling parameter is taken from Ref. [14], $2\gamma/g\mu_B = -1.18 \cdot 10^{-24}$ Tm^3. In the presence of structural asymmetry (such as asymmetry in the confinement potential of a quantum well) the electrons will also experience the Rashba SO field, given by [12]

$$\vec{B}_R = C_R\left[\hat{x}k_y - \hat{y}k_x\right]. \tag{5.4}$$

The value of the C_R is different for different structures, since it is a geometry dependent parameter. Notably, for quantum wells in GaAs it can produce a

contribution to the total effective SO field that has the same order of magnitude as the linear Dresselhaus term [14].

An electron in such material experiences the vector sum of all these contributions to the SO field, and its spin is precessing accordingly. In the case with also an externally applied magnetic field present, the spin precesses in the vector sum of the total SO field and the external field. The principal difference between the effective magnetic field from SO interaction and the externally applied magnetic field is that the SO field does not affect the motion of the electron and only interacts with the spin (when neglecting higher order relativistic corrections). An externally applied magnetic field, however, also couples to the electron orbit and induces cyclotron motion for the mobile electrons in the material. This effect of the external B-field on the electron motion can be nearly absent for electron states with strong quantum confinement. The confinement energy can then forbid the orbits to form, as for example in the case of a magnetic field in the plane of a narrow quantum well). The formation of cyclotron orbits is further discussed in the Methods section.

5.3 Method

Our numerical approach is based on a semi-classical picture for the electron motion in the material. Electrons are assumed to move with Fermi velocity (independent of the momentum direction). They never escape the region of the interest as they scatter on the walls elastically. For smooths wall this will be specular scattering, while elastic scattering on a wall with surface roughness is modeled as elastic scattering in a random direction. Electrons also have a have probability to scatter inside the volume of interest, which is defined by the mobility. This approximation for electron motion is valid for motion in directions without quantum confinement, and for the case of $E_F \gg kT, \Delta E_{Zeeman}, E_{SO}$. For a more detailed explanation of approach, the basic model and assumptions were refer to *Chapter 4* and our previous work [15, 16]. This work and related results from the Folk group [17, 18] on modeling the spin dynamics in confined structures of material with a two-dimensional electron system showed that this approach is reliable and efficient.

Here we focus on the modeling of the temporal evolution of spin polarization in a three-dimensional electron ensemble that is ballistically confined in a wire (typical dimension is 1 μm by 1 μm by 200 μm). The total SO field that electrons experience consists of the bulk Dresselhaus term (Eq. 5.1) and the Rashba term

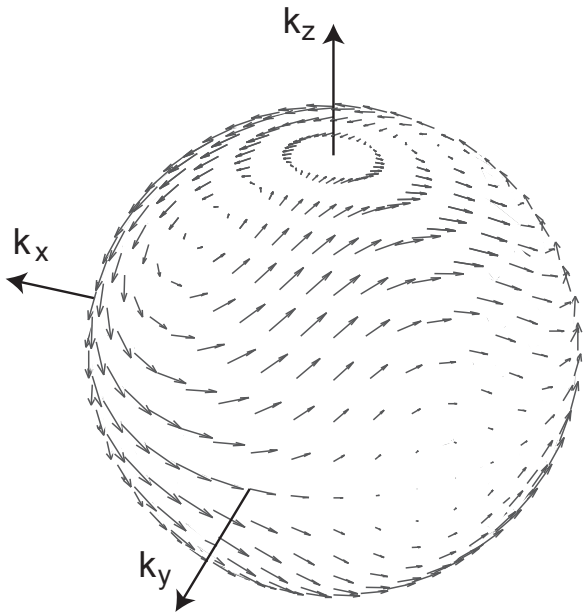

Figure 5.1: The total spin-orbit field experienced by electrons with the Fermi velocity, for the case where the contributions $|\vec{B}_R| = |\vec{B}_D^{bulk}|$ for electrons that move in the xy-plane. This leads to $B_{SO}^{total} = 0$ for electrons that move in [-110] and [1-10] direction, and for some directions with non-zero k_z.

(Eq. 5.4). Inclusion of the bulk Dresselhaus term is natural, while the Rashba term for three-dimensional structures is rarely considered. Nevertheless a Rashba-like SO field also appear for structures without a pure two-dimensional nature, since the necessary requirement for heaving such SO present is hidden in the asymmetry of the potential. A Rashba term should be effective in all cases with a unidirectional electric field in the volume of interest.

In this case, exact cancelation of SO terms is also still possible for specific directions of electron motion. The potential advantage of using three-dimensional structures lies in the possibility of strongly tuning the cancelation of Rashba and Dresselhaus terms by tuning the electron density (which is easy to achieve for the optical experiments in which spin dephasing anisotropy (SDA) was observed [10]). It comes from the fact that B_D is proportional to k^3, while the B_R is linear in k, and the value of k_F in the system is defied by the total electron density. An example of the engineered cancelation of SO field is presented in Fig. 5.1.

For the case with no external magnetic field the modeling of such a three-dimensional wire is not very much different from the two-dimensional case (*Chap-*

ter 4). However, the presence of such field with a magnitude that that is of interest in the experiments requires to include the cyclotron motion of an electron. At the same time, the calculation should keeping track of the spin precession in the total field (external and SO fields), and check for momentum scattering on the walls of the wire. This extension thus makes the calculations for the 3D case computationally much more demanding than the 2D case. However, the simplicity of this numerical approach on a complex physical situation still has counts as an advantage in comparison with efforts that aim at analytically solving this model.

A necessary requirement for observing SDA in three-dimensional wire is (as for the 2D case) that the spin precession length is smaller than the transverse wire dimension. For our simulations we kept the material parameters at values that yield a spin precession length of about $\sim 10\mu$m in zero external field. In the numerical experiments we vary the wire orientation in the xy-plane. This is the primary parameter in the search for SDA, that should appear as T_2^* values that depend on wire orientation. We also vary the electron density, strength of the coupling parameter for the Rasba SO, and the value of the external magnetic field.

5.4 Results

We expected non-zero SDA results for 3D wires (based on extrapolating our findings for the 2D case) that would show a maximum T_2^* for a wire orientation along the direction with the smallest SO fields (all in xy plane, see for example Fig. 5.1) A wire orientation perpendicular to this direction should then give a minimum T_2^*. For cancelation of B_D by a B_R term as in Fig. 5.1 this would lead to a maximum T_2^* for wires along the [-110] direction, and minimum T_2^* for the [110] orientation. However, while Fig. 5.1 represents the magnitude and sign for B_D and B_R that we estimate for the experimental situation, the expected SDA is then in fact opposite to what was observed in the experiments [10] (both 2D and 3D wires had a peak in T_2^* for wires in the [110] direction). This discrepancy is further explored in the Section.

Note that in the three-dimensional case the direction of the SO field cancelation is opposite to that of the two-dimensional case (Fig. 5.2) if we focus only on motion in xy plane. This comparison is for identical signs for the underlying Dresselhaus and Rashba terms, but the symmetry changes because the effective sign for the Dresselhaus contribution gets reversed (see Eq. (5.1), for the 2D case

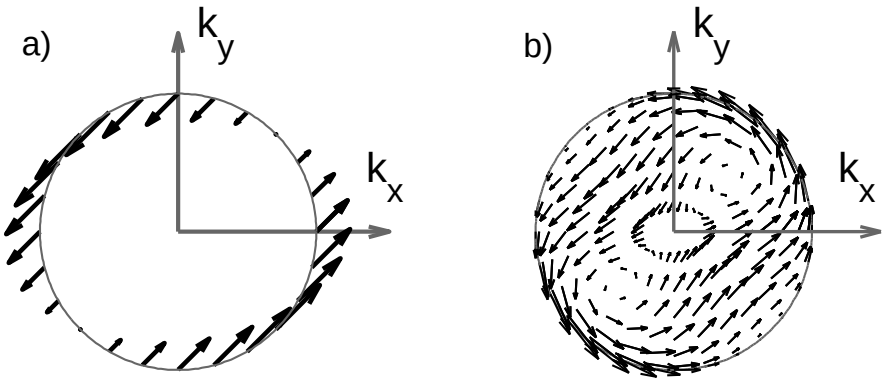

Figure 5.2: (a) A schematic representation of the spin-orbit (SO) fields as an effective magnetic field for selected points (Fermi circle with radius k_F in the k_xk_y-plane) in a two-dimensional k-space. The SO field is the sum of the Rashba field and linear Dresselhaus field for the two-dimensional case with exact cancelation for k-vectors in [110] direction. (b) A similar representation for selected points in a three-dimensional k-space (top view onto a Fermi sphere with radius k_F), with the total field as the sum of the Rashba field and the bulk (cubic) Dresselhaus field for the three-dimensional case. Both the magnitude and direction of the total SO field are depicted as arrows. For the 2D and 3D case the Rashba term has the same sign, while the Dresselhaus SO field is reversing its sign (in the xy-plane). This sign flip is due to the fact that for the 2D case $\langle k_z^2\rangle \gg k_x^2 + k_y^2$, while the dominant motion in the xy plane for the 3D case is carried by electrons with $k_z \approx 0$ and $k_z^2 \approx 0$.

$\langle k_z\rangle = 0$ and $\langle k_z^2\rangle \gg k_x^2 + k_y^2$, while the dominant motion in the xy plane for the 3D case is carried by electrons with $k_z \approx 0$ and $k_z^2 \approx 0$). Also the $SU(2)$ symmetry [5] for the thee-dimensional bulk case is not applicable.

Results for zero external magnetic field

We start the discussion of results with the simulations for zero external magnetic field. Here the electrons move randomly in the wire and experience specular scattering on the edges and random scattering inside the wire. The spin ensemble is prepared in a state that points in the the [001] direction.

Calculated time traces with the expectation value for spin polarization in the ensemble are presented in the Fig. 5.3. As in *Chapter 4* we plot $\langle S_r\rangle$ (spin expectation value in the direction that it is maximum) to account for collective spin precession, but for this plot it overlaps with results for $\langle S_z\rangle$. The spin expectation

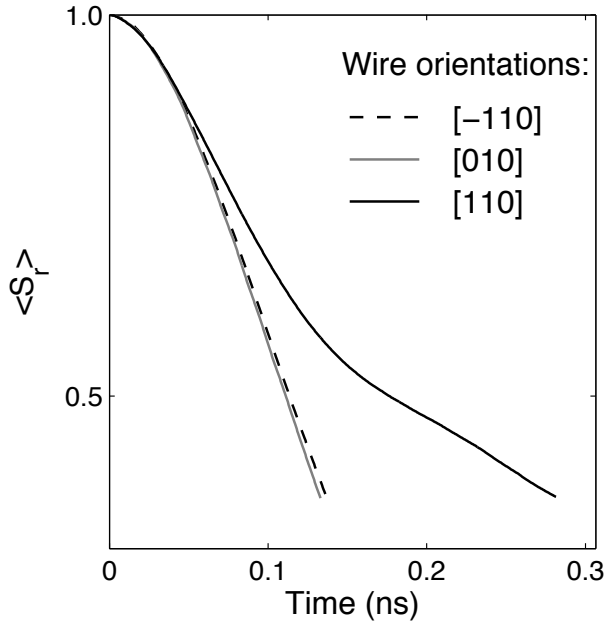

Figure 5.3: Ensemble spin expectation value $\langle S_r \rangle$ as a function of time for different wire orientations.

value for an ensemble is decaying in time due to precessional dephasing in the SO fields. For wires along the [110] direction the spin dephasing is clearly suppressed in comparison with wire in the other directions.

We investigated the T_2^* values for a range of wire orientations (Fig. 5.4(a)). The wire direction [110] yields the slowest spin dephasing for an electron spin ensemble. Notably, this is consistent with the experimental observations [10], but opposite to our qualitative expectation that the directions on the Fermi sphere with near-zero SO fields determine the direction in which wires give the longest T_2^* values (as for a 2D case). Thus, this qualitative argument can not explain the results for the 3D case (see Fig. 5.2).

To make a connection to the standard motional narrowing picture [19] we change the scattering on the edges of gthe wire to non-specular (scattering in a random direction). Results for this case are presented in Fig. 5.4(b). Now the simulations do give the longest T_2^* values for wires in the [-110] direction, and minimal values for [110] oriented wires. These results are indeed consistent with the motional narrowing mechanism, and simply show the longest T_2^* for the wire direction where the spin-orbit field is the smallest for electron motion along the wire (and vice versa). Dephasing by the highest SO field values during motion

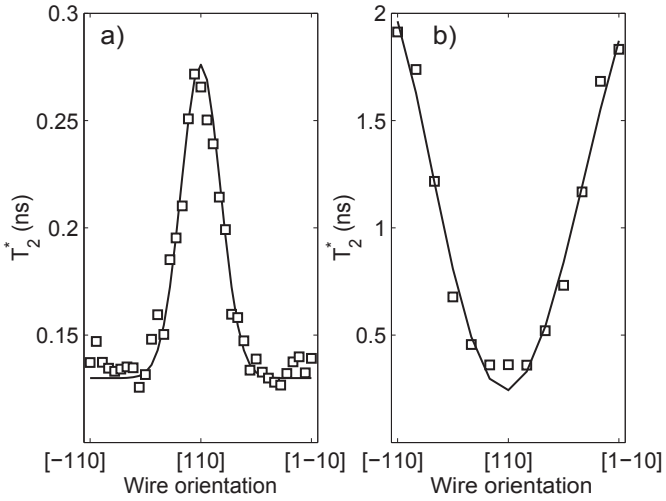

Figure 5.4: The spin-dephasing time T_2^* of a spin ensemble plotted as a function of the wire orientation. (a) For electrons with specular momentum scattering on the edges of the wire. (b) For electrons with non-specular momentum scattering on the edges of the wire.

transverse to the wire direction is suppressed by frequent momentum scattering on the walls.

Additional checks that we performed include specular scattering for a wire with transverse dimensions of 0.7 μm by 1.4 μm. This gave results very close to the SDA as for specular scattering in the wire with 1 μm by 1 μm transverse dimensions. Further, we checked that setting the Rashba term to zero for the case of specular scattering gave $T_2^* \approx 0.33$ ns, with almost no dependence on wire orientation.

From comparing these cases we conclude that for the case of specular scattering the spin dephasing anisotropy is not due to the confinement enhanced motional-narrowing effect. Instead, it must be due to an interplay between repetitive ballistic electron trajectories (from frequent wall collisions) in the wire and the anisotropy in the spin orbit fields. The mechanism then has similarities with the phenomenon of ballistic spin resonance that can occur in wires based on 2D electron systems [13]. However, here it can already occur when the width of the wire is well below the spin precession length. Studies that can confirm this picture are in progress.

Since the scattering mechanism for wire edges in the real devices is more likely to be specular (due to screening the potential of the edges is smoothed) we further

focus only on this type of the scattering.

It is useful to attribute a numerical value to the SDA. For our further studies we define it is as the ratio between the spin dephasing time in a wire along the [110] direction and a wire along the [-110] direction.

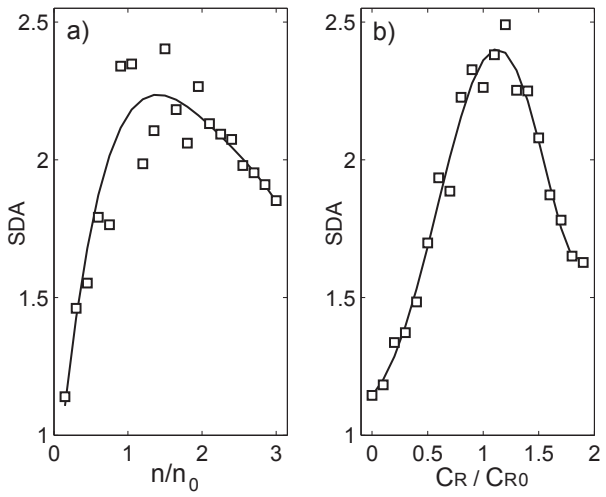

Figure 5.5: Spin dephasing anisotropy SDA as a function of simulation parameters. Data points from the numerical experiments are supported by a guide to the eye (solid line). (a) Electron density dependence of the SDA. (b) Dependence of SDA on the relative strength of the Rasha SO field (normalized to the value which yields $|B_R| = |B_D^{bulk}|$ in the xy-plane).

To investigate the link between the SDA and exact cancelation of the SO field along the direction perpendicular to the wire we vary two simulation parameters. Results from varying the density of electrons (and thereby k_F) in the wire are presented in Fig. 5.5(a). We observe a maximum SDA for the value of the electron density which leads to exactly zero SO field in the direction [-110]. This provides further evidence that the symmetry of the SO fields indeed underlie the SDA. This is further confirmed by results for the SDA as a function of the strength of the Rasha spin-orbit coupling [Fig. 5.5(b)]. We see here similar behavior as in Fig. 5.5(a). The SDA weakens when deviating from values which give exact cancelation of the two SO fields for electrons with k-vectors in the [-110] direction.

Magnetic field dependence

We now turn to discussing the results of calculations where the effects of an external magnetic field are included in the model. A first remark is that we

observed that the SDA as in Fig. 5.4 collapses in fields of about 1 Tesla, for any direction of the field. At the same time, we observe that analysis of this collapse is complicated because a richer structure in the dependence of T_2^* on wire orientation appears.

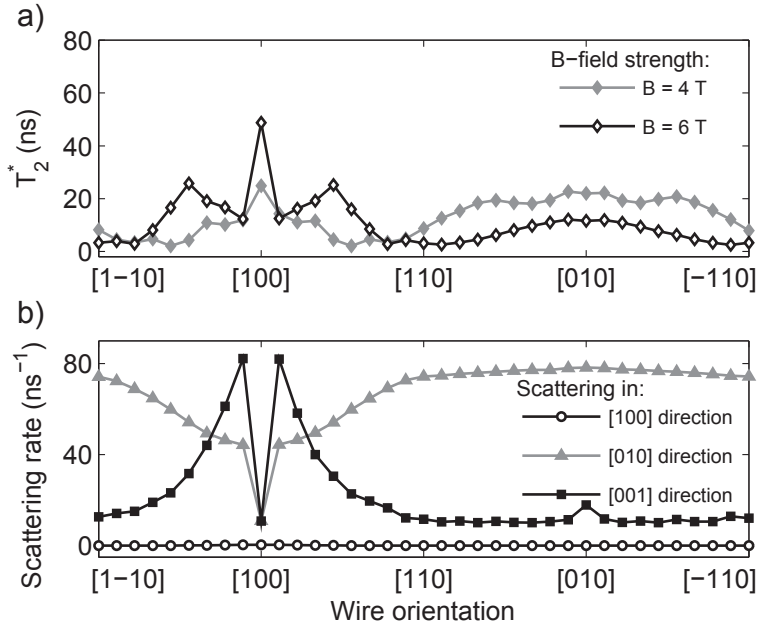

Figure 5.6: Spin dephasing time and momentum scattering in wires in an external magnetic field. (a) The spin dephasing time T_2^* for different wire orientations at 4 Tesla and 6 Tesla. (b) The momentum scattering rate for motion in specific directions at B=4 Tesla. The scattering rate represents the amount of scattering for motion in both (positive and negative) directions in the specified direction.)

This is illustrated in Fig. 5.6, with results for a B-field along the [100] direction. Upon increasing the external field to a few Tesla, the typical dephasing times increase since the relative strength of the SO fields is getting smaller. For ideal alignment of the field with a wire (*i.e.* a wire in the [100] direction) there is a sharp peak in the T_2^* which we attribute to the formation of stable cyclotron orbits that are not disturbed by wall collisions. The electrons can then move freely along the wire with very small probability to scatter on the edge, and such trajectories preserve the averaged spin orientation. This interpretation is supported by the study of scattering rates that is presented in Fig. 5.6(b).

As soon as the wire orientation deviates a small amount from this ideal alignment, the cyclotron orbits are no longer closed, but turn into skipping orbits on the walls. This comes along with frequent random scattering and differences in

the precession dynamics within the electrons ensemble (observed as much lower T_2^* values). In this regime the external magnetic field is dominating the motion of electron trajectories, and this in turn governs the spin dephasing.

5.5 Conclusions

We presented a numerical tool for studying the temporal evolution of spin ensembles in micronscale structures of bulk GaAs material. Our modeling tool is based on a semiclassical picture for the electron spin in the material. Simulations with this tool show spin dephasing anisotropy (SDA) for electron ensembles in quasi-ballistic wires. These calculations serve as a theoretical background for effects which have been observed experimentally. We quantify the spin dephasing times and SDA for material parameters as in the experiment, and find reasonable agreement.

By comparing results for specular and non-specular momentum scattering on the edges of the wires we find that the spin dephasing anisotropy in 3D wires with specular scattering arises due to a different mechanism than confinement-enhanced motional narrowing. We attribute the observed SDA to a new mechanism that can be pictured as ballistic spin resonances that occur due to the interplay between repetitive scattering trajectories and the symmetries in the spin-orbit fields. Notably, this already occurs when the spin precession length is smaller than the transverse wire dimensions. Our SDA findings agree with the experimental results (for which can indeed expect specular scattering), while the motional narrowing picture does not.

We also studied the effect of an external magnetic field on a spin polarized electron ensembles in a wire. For values of the magnetic field where the cyclotron radius is smaller than the wire width the field dominates that character of the electron trajectories and the amount of wall scattering. In turn, this is decisive for the spin dephasing time. These results are very sensitive to the alignment of the wire with respect to the magnetic field and the crystallographic axis.

We thank S. Artyukhin and A. Rudavskyifor help and valuable discussions and acknowledge the support of the High Performance Computing Center at the University of Groningen.

References

[1] M. I. D'yakonov and V. I. Perel', Sov. Phys. Solid State **13**, 3023 (1972).

[2] R. Winkler, *Spin-Orbit Coupling Effects in Two-Dimensional Electron and Hole Systems*, Springer Tracts in Modern Physics Vol. 191 (Springer, Berlin, 2003).

[3] J. D. Koralek, C. P. Weber, J. Orenstein, B. A. Bernevig, Shou-Cheng Zhang, S. Mack, and D. D. Awschalom, Nature (London) **458**, 610 (2009).

[4] N. S. Averkiev, L. E. Golub, and M. Willander, J. Phys.: Condens. Matter **14** R271 (2002).

[5] B. Andrei Bernevig, J. Orenstein, and Shou-Cheng Zhang, Phys. Rev. Lett. **97**, 236601 (2006).

[6] M. Duckheim and D. Loss, Phys. Rev. B **75**, 201305(R) (2007).

[7] M. Duckheim, D. L. Maslov, and D. Loss, Phys. Rev. B **80**, 235327 (2009).

[8] M. Duckheim, D. Loss, I. Adagideli, and P. Jacquod, Phys. Rev. B **81**, 085303 (2010).

[9] A. W. Holleitner, V. Sih, R. C. Myers, A. C. Gossard, and D. D. Awschalom, Phys. Rev. Lett. **97**, 036805 (2006); A. W. Holleitner, V. Sih, R. C. Myers, A. C. Gossard, and D. D. Awschalom, New J. Phys. **9**, 342 (2006).

[10] S. Z. Denega, T. Last, J. Liu, A. Slachter, P. J. Rizo, P. H. M. van Loosdrecht, B. J. van Wees, D. Reuter, A. D. Wieck, C. H. van der Wal, Phys. Rev. B **81**, 153302 (2010).

[11] G. Dresselhaus, Phys. Rev. **100**, 580586 (1955).

[12] R. H. Silsbee, J. Phys. Condens. Matter **16**, R179 (2004).

[13] S. M. Frolov, S. Lüscher, W. Yu, Y. Ren, J. A. Folk, and W. Wegscheider, Nature (London) **458**, 868 (2009).

[14] J. B. Miller, D. M. Zumbuhl, C. M. Marcus, Y. B. Lyanda-Geller, D. Goldhaber-Gordon, K. Campman, and A. C. Gossard, Phys. Rev. Lett. **90**, 076807 (2003).

[15] E. J. Koop, B. J. van Wees, C. H. van der Wal, arXiv:0804.2968 (2008).

[16] J. Liu, T. Last, E. J. Koop, S. Denega, B. J. van Wees, C. H. van der Wal, J. Supercond. Nov. Magn. **23**, 11 (2010).

[17] S. Lüscher, S. M. Frolov, J. A. Folk, Phys. Rev. B 82, 115304 (2010).

[18] W. W. Yu, S. M. Frolov, S. Lüscher, J. A. Folk and W. Wegscheider, arXiv:1009.5702 (2010).

[19] J. Fabian, A. Matos-Abiague, C. Ertler, P. Stano, and I. Zutic, *Semiconductor Spintronics*, Acta Phys. Slov. **57**, 565 (2007).